13

Spectroscopic Microwave Dielectric Model of Moist Soils

Valery Mironov and Pavel Bobrov
Kirensky Institute of Physics Siberian Branch of the Russian Academy of Sciences
Russian Federation

1. Introduction

Microwave dielectric models (MDM) of moist soils are an essential part of the algorithms used for data processing in the radar and radio thermal remote sensing (Ulaby et al., 1986). So far, the MDMs for moist soils developed in (Wang & Schmugge, 1980; Dobson et al., 1985; Peplinski et al., 1995, a, b) have become a routine mean for creating processing algorithms, which concern radar and radio thermal remote sensing of the land. In our recent publications (Mironov et al., 2002; Mironov, 2004; Mironov et al., 2004; Mironov et al. 2009 a, b) the error of dielectric predictions for moist soils has been noticeably decreased due to taking into account, on a physical bases, the impact of bound soil water (BSW). This is an essential distinction of the dielectric models developed in (Mironov, et al. 2002; Mironov, 2004; Mironov et al., 2004; Mironov et al., 2009 a, b) from the previous dielectric models, which are mainly of regression origin when it concerns impact of BSW. In these works, the MDM for moist soil was worked out using an extensive continuum of experimental dielectric data, both measured by the authors and borrowed from the literature. As a result, the newly developed MDM for moist soils attained features of a physical law and ensured more accurate dielectric predictions, with the soil clay content being an intrinsic texture parameter of the soil. Further research in this area has to be aimed at broadening the ensemble of soil types, temperatures, and frequency ranges over which the new MDM can be effectively used for the radar and radio thermal remote sensing of the land, including the ground penetrating radars and TDR applications.

In this chapter, a methodology to develop physically based MDM for moist soils thawed is presented. The moist soil consists of a matrix of mineral and organic particles, air, and aqueous solutions, the latter being further referred to as soil water. It is evident that, when developing a physically based MDM, the law of wave propagation through such a mixture is the first problem to be solved.

Let us consider the propagation of plane harmonic wave in a lossy, nonmagnetic, and unbounded mixture. In this case, the wave amplitude as a function of time, t, and propagation distance, x, may be written in the form:

$$exp[i(kx-\omega t)] \tag{1}$$

where $i=\sqrt{-1}$ is imaginary unit, $k= k_0 n^* -$ wave propagation constant in a mixture, $k_0 = \omega/c -$ wave propagation constant in a vacuum, $\omega =2\pi f -$ circular wave frequency, $f -$ wave frequency, $c -$ velocity of light in a vacuum, $n^*=n+i\kappa -$ complex index of refraction (CIR), $n=Rek/ k_0 -$ index of refraction (IR), $\kappa=Imk/k_0 -$ normalized attenuation coefficient (NAC), with n^*, n, and κ being related to a mixture. The CIR is a square root of complex dielectric constant (CDC), $\varepsilon= \varepsilon'+ i\varepsilon''$:

$$n^* = \sqrt{\varepsilon} \tag{2}$$

For the real, ε', and imaginary, ε'', parts of the CDC, there will be used terms dielectric constant (DC) and loss factor (LF), respectively. According to (2), the DC and LF can be expressed through the IR and NAC and vise versa:

$$\varepsilon'=n^2 - \kappa^2, \qquad \varepsilon'' = 2n\kappa \tag{3}$$

$$n=\sqrt{\sqrt{\varepsilon'^2+\varepsilon''^2}+\varepsilon'}\Big/\sqrt{2}, \quad \kappa=\sqrt{\sqrt{\varepsilon'^2+\varepsilon''^2}-\varepsilon'}\Big/\sqrt{2}, \tag{4}$$

In general, a frequency and temperature, T, dependent CDC for a mixture containing N components can be written in the form

$$\varepsilon_s=\varepsilon_{sm}(m_1,\ldots,m_N, \varepsilon_1,\ldots, \varepsilon_N ,f,T)= \varepsilon_{sv}(v_1,\ldots,v_N, , \varepsilon_1,\ldots, \varepsilon_N, f,T) \tag{5}$$

where ε_p , m_p and v_p ($p=1,\ldots,N$) are respectively CDC, gravimetric and volumetric percentages of individual components. We consider the following individual components mixed in moist soil (Ulaby et al., 1986):

1. Mineral matrix consisting of particles of various minerals, which is characterized by gravimetric percentages of clay, C, sand, S, and silt, $L=100\%-C-S$;
2. Air contained in soil pores;
3. Bound soil water (BSW) consisting of conglomerates of water molecules bound on the surface of the soil mineral matrix;
4. Free soil water (FSW), which is located in soil pores and exists in a form of capillary aggregations;

The CDC of air is considered to be equal to one, εa=1. It has been shown (Ulaby et al., 1986) that the CDC of mineral matrix, $\varepsilon_m(C, S)$, depends on gravimetric percentages of clay, C, sand, S, and silt, 100%-C-S, being practically independent on the temperature and wave frequency. On the contrary, due to water molecules relaxation (Hasted J., 1973) the CDCs of BSW, $\varepsilon_b(f, T, C, S)$, and FSW, $\varepsilon_u(f, T, C, S)$, are dependent on frequency and temperature. In addition, these values are considered to be dependent on the soil texture parameters. The latter is justified by bound water molecules interaction with the soil mineral matrix surface and the mineral matrix impact on geometric form and size of capillary water aggregations. At the same time, we assume the CDCs of BSW and FSW to be mutually independent on their percentages, m_b and m_u. With these suggestions, the CDC of moist soil can be expressed in the form

$$\varepsilon_s(v_m, v_a, v_b, v_u, f,T) =\varepsilon_s(v_m, v_a, v_b, v_u, \varepsilon_m(C, S), \varepsilon_b(f, T, C, S), \varepsilon_u(f, T, C, S)). \tag{6}$$

As seen from (6), the assumptions made allowed to decompose the variables in (5) representing the percentages of moist soil components and consider the CDCs of individual components as parameters of a mixture dielectric model, which are in their turn dependent on frequency, temperature, and soil texture characteristics. The equation (6) suggests the CDCs of individual components to be independent on their percentages. Such mixtures can be identified as conservative, once their individual components do not affect each other. This assumption may not be true, for instance, in the case of saline soils, with the values of $\varepsilon_b(v_b, f, T, C, S)$, $\varepsilon_u(v_u, f, T, C, S)$ varying due to possible change of soil solute concentration, with the percentages v_b and v_u being changed. There have been proposed plenty of mixture models, which are discussed in (Wang & Schmugge, 1980). From all of those, the refractive mixing dielectric model (RMDM) of (Birchak, 1973)

$$(\varepsilon_s)^\alpha = \sum v_p(\varepsilon_p)^\alpha, \quad p=m, a, b, u \tag{7}$$

was used as a basis for the moist soil dielectric models suggested in (Wang & Schmugge,1980) and (Dobson et al., 1985). In formula (7), a is a constant shape factor, and the subscripts m, a, b, and u designate mineral matrix, air, bound water, and free water, respectively. As seen from (7), the RMDM meets a conservative mixture condition. In the following section, there are discussed some specific equations for the RMDMs contemporarily used.

2. Refractive mixing dielectric models

Let us consider the propagation of plane wave through a mixture using the geometrical optics approximation. Given the plane wave ray is straight line, a statistically averaged complex phase of the wave that propagated the distance L in a mixture can be written in the form

$$\left\langle n_s^* \right\rangle k_0 L = \left\langle \sum_{i=1}^{N_m} n_m^* k_0 L_{mi} + \sum_{i=1}^{N_a} n_a^* k_0 L_{ai} + \sum_{i=1}^{N_b} n_b^* k_0 L_{bi} + \sum_{i=1}^{N_u} n_u^* k_0 L_{ui} \right\rangle \tag{8}$$

In equation (8), the symbol <> designates statistical averaging over an ensemble of rays, N_m, N_a, N_b, N_u and L_{mi}, L_{ai}, L_{bi}, L_{ui} are respectively the numbers of wave paths and the distances propagated through the media of soil matrix, air, BSW, and FSW, as related to an individual cell of the soil. After statistical averaging and dividing both parts of (8) by k_0L, the moist soil CIR can be represented as follows:

$$n_s^* = n_m^* L_m^{av} + n_a^* L_a^{av} + n_b^* L_b^{av} + n_u^* L_u^{av} \tag{9}$$

where the symbols L_m^{av}, L_a^{av}, L_b^{av}, and L_u^{av} stand for the normalized by L mean wave paths in the media of soil mineral matrix, air, BSW and FSW, respectively. Assuming the wave beam to be non-divergent when propagating in the mixture, one can link the normalized mean wave paths to the volumetric contents of respective substances contained in a mixture:

$$L_p^{av} = V_p / V \tag{10}$$

where V and V_p are respectively the volumes of the mixture as a whole and the ones related to specific components contained in the mixture (p=m, a, b, and u). Finally, substituting (10) in (9) yields a refractive mixing dielectric model in the form of (7), with the shape factor, a, being equal to:

$$a = 1/2. \tag{11}$$

Following the paper (Mironov et al., 1995), we re-arrange equation (7) as follows;

$$n_s = \begin{cases} n_d + (n_b - 1)W, & W \le W_t \\ n_d + (n_b - 1)W_t + (n_u - 1)(W - W_t), & W \ge W_t \end{cases}, \tag{12}$$

$$\kappa_s = \begin{cases} \kappa_d + \kappa_b W, & W \le W_t \\ \kappa_d + \kappa_b W_t + \kappa_u (W - W_t), & W \ge W_t \end{cases} \tag{13}$$

where the volumetric soil moisture, W= V_w/ V, is a ratio of the total soil water content, V_w, to the given volume, V, of dry soil sample, W_t is the maximum bound water fraction (MBWF) in a specific type of the soil. The MBWF is such an amount of water in soil that any additional water added to the soil in access of this amount behaves as free soil water. As seen from (1), the CIR is a piecewise linear function of soil moisture, with the MBWF being a transition point in terms of slope angle between the two linear legs relating to the bound, $W \le W_t$, and free, $W > W_t$, moisture ranges. In formulas (12) and (13), the variables n_d and κ_d are respectively the IR and NAC for a dry soil. With the use of formula (7), these values can be derived in the form

$$n_d = 1 + \frac{n_m - 1}{\rho_m} \cdot \rho_d = 1 + (n_m - 1) \cdot (1 - P) \tag{14}$$

$$\kappa_d = \frac{\kappa_m}{\rho_m} \cdot \rho_d = \kappa_m \cdot (1 - P) \tag{15}$$

where ρ_m and ρ_d are the specific and bulk soil densities, respectively, P=V_a/ V_d is the soil porosity, which is equal to the ratio, of the air volume in a dry soil sample, V_a, to a total volume of dry soil sample, V_d. The RMDM was initially proposed in (Birchak, 1973), with no distinction being made between the bound and free soil water. Later (Mironov et al., 1995), it was generalized in the form given by the equation (12), (13), which made possible to distinguish between contributions in the moist soil CIR, generated by the bound and free types of soil water.

The term $(n_m^*-1)/\rho_m$ can be considered collectively as a single mineral parameter of the soil CIR. In the formulas (12)-(15), the values n^*_p=n_p+iκ_p, (p= s, m, d, b, u), W_t are understood as functions of the temperature, soil texture, and frequency: n^*_d=n^*_d(T, C ,S), n^*_m=n^*_m(T, C ,S), n^*_p=n^*_p(T, C, S,f); p=s, b, u; W_t=W_t(T, C, S).

3. Parameters of the RMDM

As seen from (12)-(13), the major advantage of the RMDM is that this model decomposed the soil moisture and soil density variables, thus reducing the problem of developing the moist soil dielectric model, as a function of temperature, soil texture, and frequency, to the one pertaining to the bound. free soil water. and to the dry soil . To obtain building blocks for developing frequency dependent dielectric models for the bound and free soil water, one has to measure, as a function of frequency, the CIRs for these types of water, as parameters in the formulas (12), (13), using the data for the moist soil CIRs measured at varying moistures and frequencies (Mironov et al., 2004).

When fitting the IRs and NACs measured as a function of soil moisture, W, with the formulas (12), (13), the values of n_d and κ_d can be obtained as the interceptions of the respective fits with the axis of ordinates at W=0. While the values of MBWF, W_t, can be identified and measured as a point at which the legs of the piecewise dependences (12), (13) intercept each other. Also, the bound and free soil water RIs and NACs can be derived from the slopes of the linear segments in the fits made with (12) and (13), respectively. As a result, the RMDM parameters n^*_d, W_t, n^*_b, and n^*_u can be obtained for a specific soil, with the texture parameters, C and S, temperature, T, and wave frequency, f, being fixed. Fitting the CIR data for moist samples measured at varying frequencies, one can obtain the spectra $n^*_b(C, S, T, f)$, and $n^*_u(C, S, T, f)$. The latter are further applied to derive the Debye relaxation parameters for both the bound and free soil water (Mironov et al., 2004). In our publications, the CIRs measured for moist soils were shown to be well fitted with the equations (12) and (13).

To quantitatively demonstrate a degree of correlation of the RMDM model with the CIRs measured for different types of soil at varying frequencies and temperatures, let us transform the equations (12) and (13) into a universal piecewise linear moisture dependences: which are able to accommodate all the data measured:

$$\bar{n}_s = \begin{cases} (\bar{n}_b - 1)\,\bar{W}_b, & \bar{W}_b \le \bar{W}_t \\ (\bar{n}_b - 1)\,\bar{W}_t + (\bar{n}_u - 1)\,\bar{W}_u, & \bar{W}_u \ge \bar{W}_t \end{cases} \tag{16}$$

$$\bar{\kappa}_s = \begin{cases} \bar{\kappa}_b\,\bar{W}_b, & \bar{W}_b \le \bar{W}_t \\ \bar{\kappa}_b\,\bar{W}_t + \bar{\kappa}_u\,\bar{W}_u, & \bar{W}_u \ge \bar{W}_t \end{cases} \tag{17}$$

where $\bar{n}_b$, $\bar{n}_u$ and $\bar{\kappa}_b$, $\bar{\kappa}_u$ are the bound and free soil water IR and NAC reduced values, respectively, $\bar{W}_t$ is the reduced value of the MBWF assigned for the universal piecewise linear RMDM. In the further analysis, we use the following numerical values for these parameters: $\bar{W}_t = 0.3$; $\bar{n}_b - 1 = 10/3$; $\bar{n}_u - 1 = 9$, $\bar{k}_b = 2/3$; $\bar{k}_u = 8/3$.

This universal RMDM gives the values of reduced RI, $\bar{n}_s$, and NAC, $\bar{\kappa}_s$:

$$\bar{n}_s(\bar{W}) = (n_s(\bar{W}) - n_d)(\bar{n}_b - 1)\bar{W}/(n_b - 1), \quad \bar{W} \le \bar{W}_t; \tag{18}$$

$$\begin{gathered}\bar{n}_s(\overline{W}) = [n_s(\overline{W}) - n_d - (n_b - 1)W_t]\overline{W}\,(\bar{n}_u - 1)/(n_u - 1), \overline{W} \geq \overline{W}_t; \\ \bar{\kappa}_s(\overline{W}) = [\kappa_s(\overline{W}) - \kappa_d]\overline{W}\bar{\kappa}_b / \kappa_b\ , \quad \overline{W} \leq \overline{W}_t; \\ \bar{\kappa}_s(\overline{W}) = [\kappa_s(\overline{W}) - \kappa_d - \kappa_b W_t]\overline{W}\bar{\kappa}_u / \kappa_u\ , \ \overline{W} \geq \overline{W}_t\end{gathered} \tag{19}$$

as a function of the reduced soil moistures,

$$\begin{gathered}\overline{W} = W(\overline{W}_t / W_t)\ , \qquad W \leq W_t \\ \overline{W} = \overline{W}_t + W - W_t \quad , \quad W \geq W_t\end{gathered} \tag{20}$$

To transform the measured IR, n_{sm}, and NAC, κ_{sm}, data as a function of the measured moistures, W_m, to a respective universal piecewise linear RMDM, the following steps have to be performed. First, fitting these data with the equations (12), (13) yields the measured values of the IR, NAC, and MBWFs related to the dry soil, bound and free soil water, that is, n_{dm}, n_{bm}, n_{um}, , κ_{dm}, κ_{bm}, κ_{um}, , and W_{tm}. Second, using these values, together with the values $\bar{n}_b$, $\bar{n}_u$, $\bar{k}_b$, $\bar{k}_u$, and $\overline{W}_t$, and applying the formulas (18), (19), and (20), the experimental values of the reduced RI, $\bar{n}_{sm}$, and NAC, $\bar{\kappa}_{sm}$, can be found, as well as the reduced soil moistures, $\overline{W}_m$. As a result, any IR and NAC data measured as a function of moisture for a given specific type of soil, frequency, and temperature can be presented with the formulas (18), (19), and (20) in a form of the universal piecewise linear RMDM.

With this approach, we analyzed the IR and NAC data measured for moist soils, which are available in the literature, to clear up whether the RMDM can be treated as a physical law and to estimate the error of this model with regard to the total experimental data set analyzed.

The IR and NAC experimental data attained for some soils at the temperatures of 20°C to 25°C, are shown in the form of the universal RMDM in Figures. 1 and 2. The soil texture classes for these soils are presented in Table 1.

Order number	Texture class	Geographical location	Clay %	Sand %	MBWF	Data source. Frequencies measured
1.	F2		17.3	56.0	0.12	(Wang & Scmugge, 1980) 1.4; 5.0 GHz
2.	H7		34.7	19.3	0.21	
3.	Harlingen clay		61.0	2.0	0.42	
4.	Vernon clay loam	Mississippi State USA	28.0	16.0	0.198	
5.	Miller clay	Texas, TX	62.0	3.0	0.24	
6.	Loam	Kansas State USA	8.53	41.96	0.077	(Dobson et al., 1985) Hallikainen et al., (1985) 1.4 to 18 GHz
7.	Sandy Loam		13.43	51.51	0.112	
8.	Silt Loam		13.48	30.63	0.1	
9.	Silty Clay		47.38	5.02	0.175	

10.	Toyoura sand (S)	Kyushu province, Japan	0.3	99.3	0.0	(Miyamoto & Chikushi, 2006) 5.0 GHz
11.	Red-yellow soil (HC)		50.0	20.9	0.25	
12.	Brown forest soil (Topsoil) (LiC)		30.4	35.3	0.12	
13.	Brown forest soil (Subsoil) (HC)		61.8	7.1	0.26	
14.	Andisol (Miyazaki) (SCL)		18.9	61.5	0.24	
15.	Heavily loamy chernozem	Altai Krai, Russia	48.2	61.8	0.158	(Komarov & Mironov, 2000; Rychkova, 1997) 0.6 to 1.43 GHz
16.	Loamy chernozem		31.28	68.72	0.113	
17.	Middle loamy chernozem		35.0	65.0	0.07	
14.	Meadow chernozem		17.12	82.88	0.05	
18.	Chestnut loam soil		13.0	87.0	0.036	
19.	Silt Loam	Krasnoyarsk Krai			0.08	(Lukin et al., 2008) 0.5 to 10 GHz
20.	Shrub tundra soil	Alaska State USA			0,16	(Savin et al., 2007) 1.0 to 16 GHz

Table 1. Soil texture classes measured.

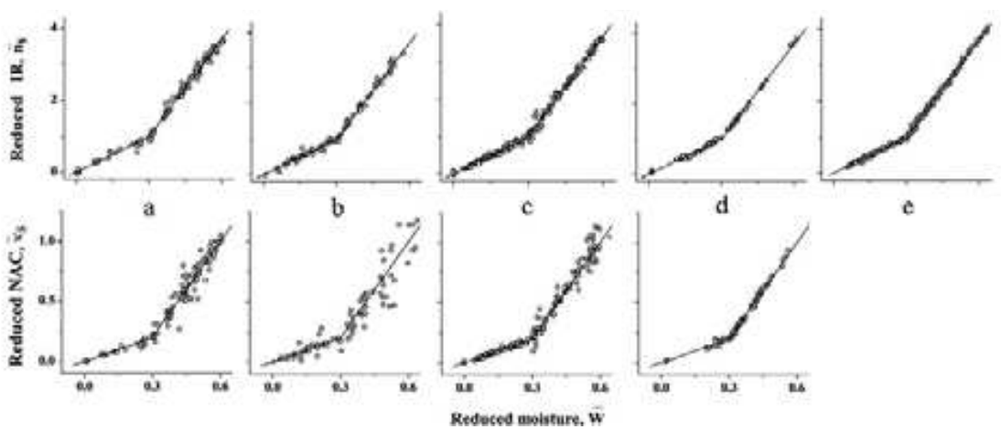

Fig. 1. Measured RI and NAC presented as values reduced with equations (18), (19) versus soil moistures reduced with formula (20). The IRs and NACs assigned for the universal piecewise linear RMDM are as follows: $\overline{W_t} = 0.3$; $\bar{n}_b - 1 = 10/3$; $\bar{n}_u - 1 = 9$, $\bar{k}_b = 2/3$; $\bar{k}_u = 8/3$. Figures from (a) to (e) pertain to the texture classes shown in Table 1: a) Soils 6 to 9; b) Soils 1 to 5; c) Soils 15 to 19; d) Soil 20; e) Soils 10 to 14.

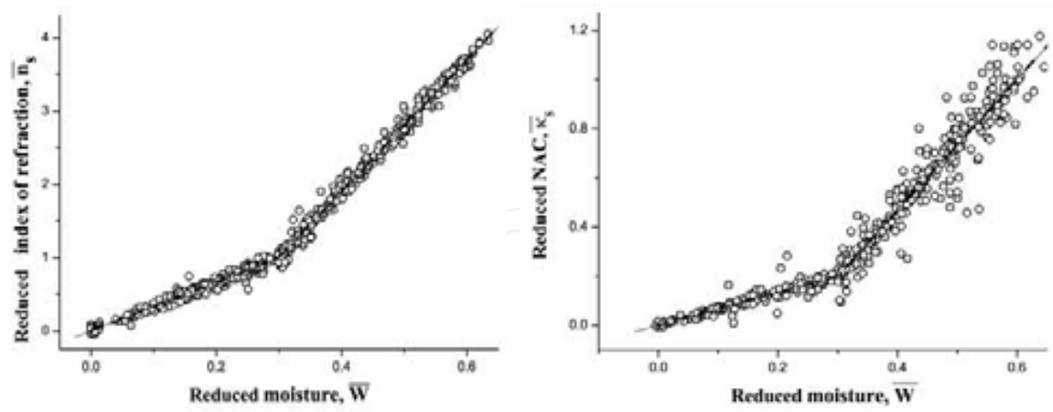

Fig. 2. The measured RI and NAC as a function of moisture presented in the form of the reduced RMDM equations (16)-(20). The data represent all the texture classes shown in Table 1. The correlation coefficients for IR and NAC, R_n and R_κ, are equal to: $R_n^2 = 0.996$, $R_\kappa^2 = 0.966$.

As seen from Figures. 1 and 2, the IR and NAC for the soils listed in Table 1, which represents a wide ensemble of textures and geographical locations, proved to be well correlated with those given by the RMDM. Taking into account a broad variety of measured soil types and frequencies, the RMDM can qualify to be treated as a general physical law, which describes, according to (1), wave propagation velocity, $v=c/n$, and amplitude attenuation coefficient, $k_0\kappa$, dependence on soil moisture. At this moment, it is worth noticing that, in regression dielectric models of (Wang&Schmugge, 1980) and (Dobson et al., 1985), the index of power, α, in the mixing formula (7) was defined as α =1 and α=0.65, respectively, which are other then the value of α =0.5 substantiated by the analysis conducted in Figure 1 and 2.

Given the RMDM parameters are obtained in some frequency range through fitting (12) and (13) to the soil IR and NAC data measured, the IR and NAC frequency spectra bor both the bound and free soil water become available, as well as those for the DC, ε', and LF, ε'', (see formula (3)), for further consideration as a function of soil texture parameters. Taking into account the formulas in (3). The same is true with regard to the soil water DCs, ε'_b and ε'_u, and LFs, ε''_b and ε''_u, pertaining to the bound and free water types, respectively. From the analysis conducted, follows that the RMDM can be applied to predict the DC and LF of moist soisl as a function of moisture, using the equations (12), (13), provided the DCs and LFs for the dry soil, bound and free soil water have been derived from the moisture dependences measured for a specific soil, at given temperatures and frequencies.

In spite of the fact that the RMDM proved applicable to the soil types on a broad scale, the soil dielectric data base developed on the basis of the RMDM would take an excessive amount of laboratory dielectric measurements, as the domain of wave frequencies, soil textures, and temperatures is too large for such a project to be ever completed. Hence, further parameterizations are needed to bring the RMDM into practical usage. In the next section, based on the Debye dipole relaxation laws, the parameterization of soil water spectra is considered.

4. Frequency dependent RMDM

To parameterize the soil water dielectric spectra, one has to be sure that these related to both the bound and free soil water types follow the Debye dipole relaxation law, as is the case for the water solutions out of the soil (Hasted, 1973). The Debye relaxation formula for the CDC has (Ulaby, 1986) the following form:

$$\varepsilon'_p + i\varepsilon''_p = \left(n_p^*\right)^2 = \varepsilon_{p\infty} + \frac{\varepsilon_{p0} - \varepsilon_{p\infty}}{1 - i2\pi f\tau_p} + \frac{i\sigma_p}{2\pi f\varepsilon_r} \tag{21}$$

where ε'_p ε''_p are DC and LF for water, p is any one of b, u,; ε_{p0} and $\varepsilon_{p\infty}$ are the low- and high- frequency limit dielectric constants, τ_p is the relaxation time, and σ_p is the ohmic conductivity, each specific to the different forms of soil moisture. Finally, ε_r = 8.854 pF/m is the DC of vacuum.

The DC and LF in (21) as a function of circular frequency ω:

$$\varepsilon'_p(\omega) = \varepsilon_{\infty p} + [\varepsilon_{0p} - \varepsilon_{\infty p}]/[1 + (\omega\tau_p)^2], \tag{22}$$

$$\varepsilon''_p(\omega) = \left([\varepsilon_{0p} - \varepsilon_{\infty p}]/[1 + (\omega\tau_p)^2]\right)\cdot \omega\tau_p + (\sigma_p\tau_p/\varepsilon_r)/\omega\tau_p \tag{23}$$

have some characteristic features. The DC monotonically decreases with the frequency, having an inflection at the frequency of $\omega_{fp}=1/\tau_p$, which can be derived from the equation $d^2\varepsilon'_p(\omega)/d\omega^2=0$. At this frequency, the DC undergoes maximum frequency dispersion. While the LF given by (23) has maximum at $\omega = \omega_r$, which is known as the frequency of relaxation and minimum at $\omega = \omega_n$. This minimum originates due to decrease and increase with frequency decreasing of the terms $([\varepsilon_{0p} - \varepsilon_{\infty p}]/[1+(\omega\tau_p)^2])\omega\tau_p$ and $(\sigma_p\tau_p/\varepsilon_r)/\omega\tau_p$, respectively. Taking into account that these terms represent the relaxation and ohmic losses, respectively, the frequency ω_n can be treated as the frequency of transition between the ranges in which the soil water dielectric mainly has losses of relaxation or ohmic origin, respectively. Hence the frequency intervals $0<\omega<\omega_{pn}$ and $\omega_{pn}<\omega<\infty$ can be identified as ohmic and relaxation loss ranges.

The relaxation and transition frequencies can be obtained as solutions of the equation $d(\varepsilon''_p(\omega))d\omega=0$:

$$\begin{aligned}(\omega_{rp}\tau_p)^2 &= \left(1 - 2s_p + \sqrt{(1-2s_p)^2 - 4s_p(1+s_p)}\right)\Big/\left(2\cdot(1+s_p)\right),\\ (\omega_{np}\tau_p)^2 &= \left(1 - 2s_p - \sqrt{(1-2s_p)^2 - 4s_p(1+s_p)}\right)\Big/\left(2\cdot(1+s_p)\right)\end{aligned} \tag{24}$$

here $s_p = \bar{\sigma}_p/(\varepsilon_{0p} - \varepsilon_{\infty p})$, $\bar{\sigma}_p = \sigma_p\tau_p/\varepsilon_r$, is a combined parameter to characterize the relationship between the ohmic conductivity, σ_p, relaxation time, τ_p, and the range of DC dispersion, ε_{0p}-$\varepsilon_{\infty p}$, for both the bound, $p=b$, and free, $p=u$, soil water types. The equations

(24) have real values provided the combined parameter, *s*, lies in the range 0≤*s*≤(1/8). Hence, in the case of DC and LF spectra for soil water, which dielectric parameter s exceeds the value of 1/8, neither the relaxation nor the transition frequencies are observed, with the LF spectra being a function monotonically increasing with decreasing frequency.
From the equations of (24), the ranges for the relaxation and transition frequency variations as a function of the combined parameter s, can be determined as follows:

$$1/\sqrt{3}\tau_p \le \omega_{rp} < 1/\tau;; \qquad 0 \le \omega_{np} < 1/\sqrt{3}\tau_p \ . \tag{25}$$

The least and largest limits of these ranges are calculated from (24), with the values of combined characteristic being equal to *s*=1/8 (at this value, the least limit for relaxation loss range occur and largest limit for ohmic loss range) and to *s*=0 (at this value, least limit for the ohmic loss range occur and largest limit for the relaxation range). In addition, according to (24), the relaxation and transition frequencies are related to each other by the equations given below in two alternative forms:

$$\begin{gathered}\omega_{np} = (1/\tau_p)\sqrt{\left[1-(\omega_{rp}\tau_p)^2\right]/\left[1+3(\omega_{rp}\tau_p)^2\right]} \quad \text{and} \\ \omega_{rp} = (1/\tau_p)\sqrt{\left[1-(\omega_{np}\tau_p)^2\right]/\left[1+3(\omega_{np}\tau_p)^2\right]} \quad \text{or} \\ \left\{\left[\omega_{np}\tau_p\right]^2/\left[1+(\omega_{rp}\tau_p)^2\right]\right\}+\left\{\left[\omega_{rp}\tau_p\right]^2/\left[1+(\omega_{np}\tau_p)^2\right]\right\}=1/2\end{gathered} \tag{26}$$

The Debye equations (22), (23) can be recast as a pair of equations which are linear in the Debye parameters. These equations can be then solved via linear regression to yield least squares estimates of the Debye parameters. The first of the two linear equations is

$$\varepsilon'_p(f) = z_{p\sigma} - \tau_p z_{p\tau}(f) \tag{27}$$

where

$$z_{p\sigma} = \varepsilon_{p0} + \sigma_p \tau_p / \varepsilon_0 \tag{28}$$

is a constant and

$$z_{p\tau}(f) = 2\pi f \varepsilon''_p(f) \tag{29}$$

is a reduced variable, which is supposed to be calculated from dielectric measurements. A linear regression with regard to the measured pairs (ε'_p, $z_{p\tau}$) of (27) yield the estimates of the parameters τ_p and $z_{p\sigma}$ from the measured pairs (ε'_p, ε''_p).
The second equation is

$$\varepsilon'_p(f) = \varepsilon_{p0} - (\varepsilon_{p0} - \varepsilon_{p\infty}) z_{p\varepsilon}(f) \tag{30}$$

where the variable

$$\frac{1}{z_{p\varepsilon}(f)} = 1 + \frac{\varepsilon''_p(f)/2\pi f\tau_p}{z_{p\sigma} - \varepsilon'_p(f)} \tag{31}$$

is thought to be known from measurements, with the values of τ_p and $z_{p\sigma}$ having been obtained from the previous regression with the use of (27). At this point, all four Debye parameters can be found using the values of τ_p, $z_{p\sigma}$, ε_{p0}, and $(\varepsilon_{p0}$- $\varepsilon_{p\infty})$ attained from the regressions. The linear fitting of the data measured for $\varepsilon'(f)$ and $\varepsilon''(f)$ with the use of (27) and (30) also provide correlation coefficients and standard deviations to estimate compliance between the measured data and the fitting ones calculated with the Debye equations (22), (23).

To universally represent various dielectric spectra of soil water measured for bound or free soil water, different types of soils and temperatures, The linear functions (27) and (30) representing the Debye equation (22), (23) can be can be modified in a universal linear function:

$$\bar{\varepsilon}'_{pj}(f) = 1 - \bar{z}_{pj}(f) \tag{31}$$

where $\bar{\varepsilon}'_{pj}(f)$ and $\bar{z}_{pj}(f)$ are the reduced DCs and frequencies which can be obtained after some algebraic manipulations performed with the pairs (27), (29) and (30), (31):

$$\begin{gathered}\bar{z}_{p1}(\omega) = \left[\tau_p \omega \varepsilon''_p(\omega) - (\varepsilon_{0p} + \bar{\sigma}_p)\right] / \left[\varepsilon_{0p} - \varepsilon_{\infty p}\right] \\ \bar{\varepsilon}'_{p1}(\omega) = \left[\varepsilon'_p(\bar{z}_{p1}(\omega)) - \varepsilon_{\infty p}\right] / \left[\varepsilon_{0p} - \varepsilon_{\infty p}\right]\end{gathered} \tag{32}$$

$$\begin{gathered}\bar{z}_{p2}(\omega) = \left[\varepsilon_{0p} + \bar{\sigma}_p - \varepsilon'_p(\omega)\right] / \left[\varepsilon_{0p} + \bar{\sigma}_p + (\varepsilon''_p(\omega)/\tau_p\omega) - \varepsilon'_p(\omega)\right] \\ \bar{\varepsilon}'_{p2}(\omega) = \left[\varepsilon'_p(\bar{z}_{p2}(\omega)) - \varepsilon_{\infty p}\right] / \left[\varepsilon_{0p} - \varepsilon_{\infty p}\right]\end{gathered} \tag{33}$$

The values j =1 and j=2 in (32), (33) correspond to the pairs (26), (29) and (30), (31), respectively.

As a result, the equation (30) in conjunction with the expressions (32), (33) can universally represent any DC, $\varepsilon'_p(f)$, and LF, $\varepsilon''_p(f)$, spectra for both the bound, $p=b$, and free, $p=u$, soil water measured for a specific type of soil, at a given temperature, provided these spectra follow the Debye equation (21). From equations (22), (23), (32), (33) follow that the reduced functions $\bar{\varepsilon}'_{p1}(f)$, $\bar{\varepsilon}'_{p2}(f)$ and their arguments $\bar{z}_{p1}(f)$, $\bar{z}_{p2}(f)$ are defined across the same segment from zero to unit, [0,1].

Substituting the values of $\varepsilon'_p(\omega)$ and $\varepsilon''_p(\omega)$ given by the formulas (22) and (23) in the expressions for the reduced frequencies $\bar{z}_{p1}(f)$ and $\bar{z}_{p2}(f)$ of (31), (32), we come up with the following simple formula:

$$\bar{z}_{p1}(f) = \bar{z}_{p2}(f) = \bar{z}_p(f) = (\omega\tau_p)^2 \Big/ \left(1 + (\omega\tau_p)^2\right) \tag{34}$$

which can be applied only in the case of formal transforming the equations (27), (28) and (30), (31) to the equations (31), (32), and (33), but not for fitting the equations (31), (32), and (33) to the DC and LF data measured. In addition, using the expressions (25) and (34) and the eqution $\tau\omega_f$=1, we find for the reduced maximal dispersion frequency, $\bar{z}_p(\omega_f)$, and the ranges for relaxation, $\bar{z}_p(\omega_r)$, and ohmic, $\bar{z}_p(\omega_n)$, frequencies to be as follows:

$$\bar{z}_p(\omega_f) = 1/2\,; \quad 0 \le \bar{z}_p(\omega_n) \le 1/4\,; \quad 1/4 \le \bar{z}_p(\omega_r) \le 1/2\,; \tag{35}$$

When presenting the data measured in the form of reduced frequencies, one can easily identify using the formula (35) specific frequency ranges which these data belong to. These ranges appear to be dimensionless due to the respective transformation conducted with (31)-(33).

An example for the DC and LF spectra following the Debye formulas (22), (23) are shown in Figure 3. They were calculated for a sample of saline water, having solution concentration and temperature of 1.88 g/liter and 20ºC, respectively, with the use of the empirical formulas obtained in (Stogryn, 1971). In Figure 3b, the same spectra for the DC and LF reduced according to (32), (33) are plotted as a function of reduced frequency, $\bar{z}_p(f)$, calculated with (34). The following parameters of the Debye spectra (22), (23) were used (τ_u=9.27 ps ; ε_{0u}=79.44; σ_u=0.3; $\varepsilon_{\infty u}$=4,9), regarding the liquid saline water, to perform transition to reduced spectrum and frequency, as given by (32), (33). The spectroscopic parameters for saline water listed above were determined with empirical formulas of (Stogryn, 1971). Here and henceforth, we understand the low and high frequency limits as the values related exclusively to a specific Debye relaxation frequency range, within which the measured data are located and the low and high frequency limits have been determined using these data. These limits can not be understood as the values of real DCs which may occur beyond the frequencies measured. Such a situation may take place if some other relaxation processes considerably contribute in the values of real DCs, making, for instance due to the Maxwell-Wagner relaxation (Hasted, 1973), real values of ε' a lot greater then the low frequency limit, ε_0, determined via data measured for its deriving. In the range of frequencies exceeding those measured, the same understanding with regard to the high frequency limit, ε_∞, has to be used, as many other relaxation processes may also occur when moving towards the optical range of frequencies.

The vertical lines in Figures. 3a and 3b mark the maximal dispersion frequency, f_f, maximal relaxation loss frequency, f_r, and the frequency of transition from relaxation to ohmic losses, f_n, as these are given with the formulas (24) and (32), (33), to display the intermediate range of frequencies in which both the relaxation and ohmic losses are observed, as well as to show the position of maximal dispersion frequency.

As any Debye spectra can be universally presented like in Figure 3, for the spectra measured a possibility arises to align those along one and the same straight line, which makes possible not only to test whether the measured spectra belong to the Debye class, but also to monitor the position of measured spectra with regard to the Debye spectra characteristic frequencies, that is, f_f, f_r, and f_n, pictured for all the data measured in one and the same graph.

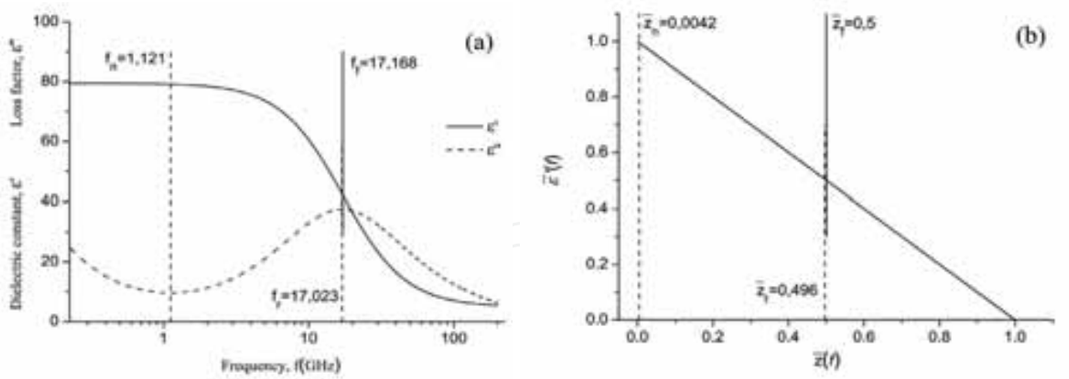

Fig. 3. Relaxation frequency spectra for the DC and LF in the case of saline liquid water, having the following values of Debye parameters: τ=9.27 ps ε_0=79.44 σ=0.3 ε_∞=4,9. a) Initial values of DC, LF and frequency; b) Reduced values of DC, LF, and frequency. With vertical lines, are marked both the real (in Fig. 3a) and reduced (in Fig. 3b) positions of the maximal dispersion frequency (f_f, and $\bar{z}_f$, solid lines), maximal relaxation loss frequency, (f_r and $\bar{z}_r$, dotted lines), and the frequency of transition to ohmic losses (f_n and $\bar{z}_n$, dotted lines). While their numerical values are placed next to the respective lines.

Fitting formulas (12) and (13) to the data for DCs and LFs as a function of moisture for the soils listed in Table 1, first, the values of DCs and LF were obtained with the technique outlined in Section I. Second, the DC and LF spectra for both the bound and free soil water obtained were fitted with the formulas (27)-(31) in order to derive the parameters present in the Debye equation (22), (23), that is the low and high frequency limits, ε_∞ and ε_0, relaxation time, τ, and conductivity, σ, regarding both types of soil water. The values thus obtained are given in Table 2.

Soil number in Table 1	7		9		19		20	
Wave frequencies measured	4 to 18 GHz		4 to 18 GHz		0.5 to 10 GHz		3.01 to 15 GHz	
Soil water type	p=b	p=u	p=b	p=u	p=b	p=u	p=b	p=u
Low frequency limit of DC, ε_{0p}	58.5	103	38.60	97.90	65.08	73.15	43.45	79.52
High frequency limit of DC, $\varepsilon_{\infty p}$	4.9	4.9	4.9	4.9	4.9	4.9	14.2±1.2	14.1±1.2
Relaxation time, τ_p(ps)	1.14	8.3	11.30	8.00	21.41	9.23	65.71	11.57
Conductivity, σ_p(S_p/m)	0.7	1.03	1.24	2.15	3.48	1.29	0,061	3,31

Table 2. Debye relaxation parameters and conductivities for some soils listed in Table 1.

We did not have the dielectric data measured for the frequencies larger then the maximal dispersion frequency, f_f, which, according to Figure 3, could make possible to derive the high frequency limit with reliable accuracy, except for the soil 20. Therefore, the value of 4.9 was preset before fitting with the formulas (27)-(31), in accordance with previously estimated data for this parameter (Mironov et al., 2004).

As follows from Table 2, the Debye relaxation parameters and conductivities relating to the bound and free water can be clearly distinguished via their magnitudes. The most important feature, seen in Table 2, is that not only the low frequency limits but also the relaxation times, as well as conductivities are found to noticeably differ from each other. It implies that, in accordance

with the analysis conducted above the maximum relaxation frequencies and transition to ohmic losses frequencies pertaining to the different types of soil water must be also different.
At the same time, in the dielectric model developed in (Dobson et al., 1985), both the bound and free water spectra were assumed to be similar to that of free liquid water existing out of soil. The mixing formula for the moist soil CDC used in (Dobson et al., 1985) can be presented as follows:

$$\varepsilon_s'(f, v_a, v_m, v_w, C, S)^\alpha = v_a(\varepsilon_a)^\alpha + v_m\varepsilon_m(C,S)^\alpha + v_w(\varepsilon_w(f)^\alpha \cdot v_w^{(\beta_1(C,S)-1)} - 1)$$
$$\varepsilon_s''(f, v_w, C, S)^\alpha = v_w^{\beta_2(C,S)} \cdot \varepsilon_w''(f, \sigma(\rho_d, C, S))^\alpha$$

were subscrip w stands for the water out of soil content and $\varepsilon_w(f)$ is a preset function characterizing the water out of soil. At that, only the power index a and the values $\beta_1(C, S)$, $\beta_2(C,S)$ and $\sigma(\rho_d,C,S)$ were adjusted to the dielectric data measured via regression analysis. While the mixing formula applied in (Wang&Schmugge, 1980) suggested the following expression for the CDC of moist soil:

$$\varepsilon_s(f, v_a, v_m, v_w, C, S) = v_a\varepsilon_a + v_m\varepsilon_m(C,S) + v_w \cdot Y \cdot \varepsilon_w(f) \quad if \quad v_w \le v_t;$$
$$\varepsilon_s(f, v_a, v_m, v_w, C, S) = v_a\varepsilon_a + v_m\varepsilon_m(C,S) + v_t \cdot Y \cdot \varepsilon_w(f) + (v_w - v_t)\varepsilon_w(f) \quad if \quad v_w \ge v_t;$$

with the values of v_t and Y being adjusted to the dielectric data measured only at 1.4 and 5 GHz. From the expressions above pertaining to the dielectric models of (Dobson et al.,1985) and (Wang&Schmugge, 1980) follows that the intrinsic properties of soil bound water spectra in terms of all the Debye relaxation parameters and conductivity could neither been measured nor taken into account on a physical ground.
The detailed consideration of both the bound and free soil water spectra measured for the soils listed in Table 2 is conducted in Figure 4 with regard to reduced spectra.

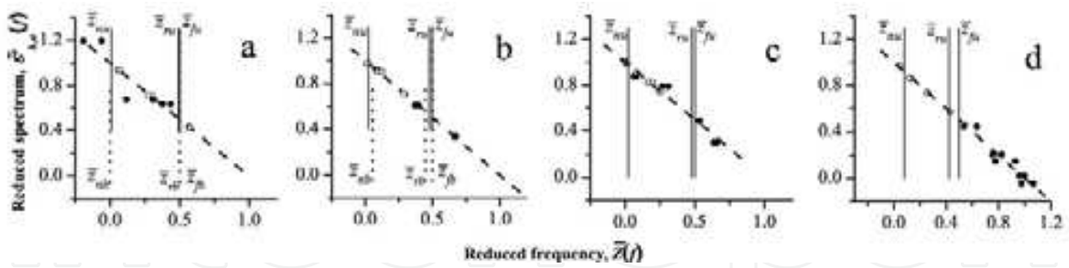

Fig. 4. Reduced spectra (slanting dotted line) for the bound and free water pertaining to some soils listed in Table 1. Position of the maximal dispersion frequency $\bar{z}_{fu} = \bar{z}_{fu} = 0.5$ is marked with vertical soilid lines. While the positions of maximal relaxation loss frequency, $\bar{z}_{rp}$, and the frequency of transition to ohmic losses range, $\bar{z}_{np}$, for the BSW, p=b, and FSW, p=u, are shown with vertical dotted and solid lines, respectively. a) Soil 7, $\bar{z}_{rb} = 0.498$, $\bar{z}_{nb} = 0.002$, $\bar{z}_{ru} = 0.49$, $\bar{z}_{nu} = 0.01$; b) Soil 9, $\bar{z}_{rb} = 0.448$, $\bar{z}_{nb} = 0.05$, $\bar{z}_{ru} = 0.478$, $\bar{z}_{nu} = 0.02$; c) Soil 19, $\bar{z}_{ru} = 0.477$, $\bar{z}_{nu} = 0.02$; d) Soil 20, $\bar{z}_{ru} = 0.421$, $\bar{z}_{nu} = 0.08$.

In contrast to the ideal reduced spectra shown in Figure 3b, some of measured data given in Figure 4 , for reduced DC, $\bar{\varepsilon}'(f)$ and frequency, $\bar{z}(f)$, fall beyond the range $0 \le \bar{\varepsilon}'(f)$, $\bar{z}(f) \le 1$. This occurred not only due to error in the spectroscopic parameters derived, which are taken from Table 2 to be used for calculating the reduced value with the formulas (32), but also because the frequencies $\bar{z}_1(f)$ and $\bar{z}_2(f)$ were calculated using in formulas (27)-(31) the data for $\varepsilon''(f)$ measured with some error. As seen from Figure 4, for both the bound and free soil water, the measured spectra for the soils 7, 9,and 19 appeared to be mainly located in the frequency range from the transition to ohmic losses frequency, f_n, to the relaxation loss frequency, f_r, with only a few frequencies exceeding the maximal dispersion frequency, f_f. For this group of soils, there is only a little difference between the characteristic frequencies related to the bound or free soil water types. Though, as to the soil 19, the intermediate frequency range, from f_n to f_r, did not appeared to be observed at all, because , in accordance with the formula (24) and data given in Table 2, the condition $0 \le s \le (1/8)$ was not met. Finally, we found the spectral properties of the bound and free soil water contained in the arctic shrub tundra soil to be quite different in terms of their frequency ranges As seen from Figure 4 d, the frequencies measured appeared to be located below and higher the respective maximal dispersion frequencies of the bound and free soil water types, respectively. In addition, there was no interim frequency interval for the bound water spectrum observed. Once in the case of this soil, the frequencies measured happened to be higher then the maximal relaxation one, the high frequency limit was measured with an acceptable error. The numerical value of this parameter is given in Table 2. As seen from Table 2, for the organic rich (95%) soil 20, the high frequency limits appeared to be about three times as large compared to the value of 4.9, which is a conventional estimate for the mineral soils (Mironov et al., 2004).
Similar to Figure 4, all the spectra measured for the soils 7, 9, 19, and 20, are presented in the reduced form in Figure 5.

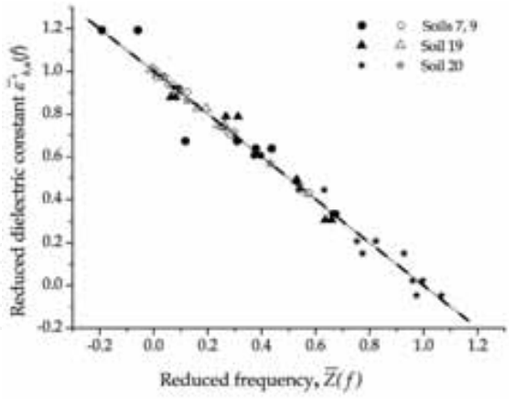

Fig. 5. Reduced spectra for both the bound (filled symbols) and free (empty symbols) soil water regarding the soils 7, 9, 19, and 20. The linear fits related to the bound and free water are drawn with dotted and solid lines, respectively. The correlation coefficient and standard deviation regarding the linear fit are equal to R= 0.988 and SD= 0.0471, respectively.

As seen from Figure 5, the data measured follow quite well the Debye relaxation formula (21) for both the bound and free soil water spectra regarding rather a broad variety of soils and frequencies measured.

The results of the analysis conducted in this Section not only substantiates the use of Debye spectra for the soil water dielectric spectra, but also propose the methodology for deriving soil water Debye parameters and conductivity. Previously, the Debye spectrum model was used in the soil dielectric models (Wang&Schmugge, 1980; Dobson et al., 1985; Mironov et al., 2004), though the applicability of this spectrum class with regard to the soil water types, especially in the case of bound water, has never been substantiated. Summing up the result of Sections 2 and 3, let us summarize the FD RMDM parameters that have to be derived from dielectric measurements to ensure the DC and LF predictions for a specific type of moist soil. As can be seen from the equations (3), (4), (12), (13), (22), (23), a certain type of moist soil, in terms of its dielectric spectra, can be completely determined via a set of the following FD RMDM parameters:

1 DC, $\varepsilon'_d(T,C,S)$, for dry soil;
2 LF, $\varepsilon''_d(T,C,S)$, for dry soil;
3 Value of MBWF, $Wt(T,C,S)$;
4 Low frequency limit dielectric constants, $\varepsilon_{0b}(T,C,S)$ and $\varepsilon_{0u}(T,C,S)$, for bound and free soil water;
5 High frequency limit dielectric constants, $\varepsilon_{\infty b}(T,C,S)$ and $\varepsilon_{\infty u}(T,C,S)$, for bound and free soil water;
6 Relaxation times, $\tau_b(T,C,S)$ and $\tau_u(T,C,S)$, for bound and free soil water;
7 Conductivities, $\sigma_b(T,C,S)$ and $\sigma_u(T,C,S)$, for bound and free soil water.

As shown in Sections 2 and 3, for a specific type of soil, all of these parameters can be derived with the use of conventional dielectric measurements of moist soils. Therefore, to be employed in the microwave remote sensing processing algorithms, the FD RMDM requires prior dielectric measurements to be carried out for a set of the individual soils involved in remote sensing data processing, and the error of dielectric predictions for each individual soil be tested. Some tests to prove the predictive power of the FD RMDM have been already conducted in (Mironov et al., 2004). Further, we use the dielectric data of (Hallikainen et al., 1985; Dobson et al., 1985, Curtis et al. 1995) to analyze prediction errors of the FD RMDM over a wide ensemble of soil types in terms of texture, as well as extended ranges of frequencies measured. Based on this analysis, the FD RMDM can be generalized to predict DCs and LFs of moist soils, with their textures being an input parameter. That frequency and texture dependent refractive mixing dielectric model (FTD RMDM) is outlined in the next section, following the results of (Mironov et al., 2009a).

5. Frequency and texture dependent RMDM

The FD RMDM was tested in (Mironov et al., 2004 a,b; Mironov et al., 2009a) with the dielectric data measured in (Hallikainen et al., 1985; Dobson et al, 1985; Curtis et al., 1995). Given the numerical values for the FD RMDM parameters (see Table 2), the ensemble of the FD RMDM formulas (3), (4), (12), (13), (22), (23) can be applied to calculate the DCs and LFs predicted with this model. Texture characteristics of the combined set of soils measured in (Hallikainen et al., 1985; Dobson et al, 1985; Curtis et al., 1995) are given in Table 3.

The ensemble of dielectric data in (Curtis et al., 1995) appeared to be incomplete, in terms of a number of moistures measured, to be applied for deriving the FD RMDM spectroscopic parameters as it was done in Sections 2 and 3. Based on the results of these sections, we suggested the FD RMDM to be applicable to the dielectric data of (Curtis et al., 1995)

measured in the domain of moistures (from nearly dry soils to field capacity values), and frequencies (from 0.45 to 26.5 GHz).

Order number	Sample code	Texture class	Clay %	Sand %	MBWF
1.	B	Sand (SP), Light Gray	0	98	0.005
2.	L	Sand (SP), Brown	0	99	0.001
3.	I	Sand (SP), White	0	100	0.001
4.	C	Silty Sand (SM), Brown	4	88	0.02
5.	E	Clayey Silt (ML), Brown	7	0	0.1
6.	K	Clayey Silt (ML), Brown; Trace of Sand	7	4	0.11
7.	F2	Loam	8.53	41.96	0.075
8.	G	Clayey Sand (SC), Dark Brown	13	55	0.07
9.	F1	Sandy Loam	13.43	51.51	0.07
10.	F3	Silt Loam	13.48	30.63	0.073
11.	D	Silty Sand, (SM), Reddish Brown	14	77	0.05
12.	H	Clay (CH), Gray	34	2	0.15
13.	F5	Silty Clay	47.4	5.02	0.17
14.	J	Silt (ML), White	54	0	0.15
15.	A	Clay (CH), Light Gray	76	2	0.28

Table 3. Texture characteristics for the soils measured in (Hallikainen et al., 1985; Dobson et al, 1985; Curtis et al., 1995).

Therefore, there was applied a procedure of fitting simultaneously the FD RMDM formulas to all the DC and LF spectra corresponding to the whole set of moistures available for each particular type of soil presented in Table 3, as was done in (Mironov et al., 2006; Mironov et al. 2009a). As an example of fitting effectiveness, in the case of soil with code D, the fits and the experimental spectra are shown in Figure 6. The results presented in this figure proves the FD RMDM ability to accurately fit the measured CDs and LFs.

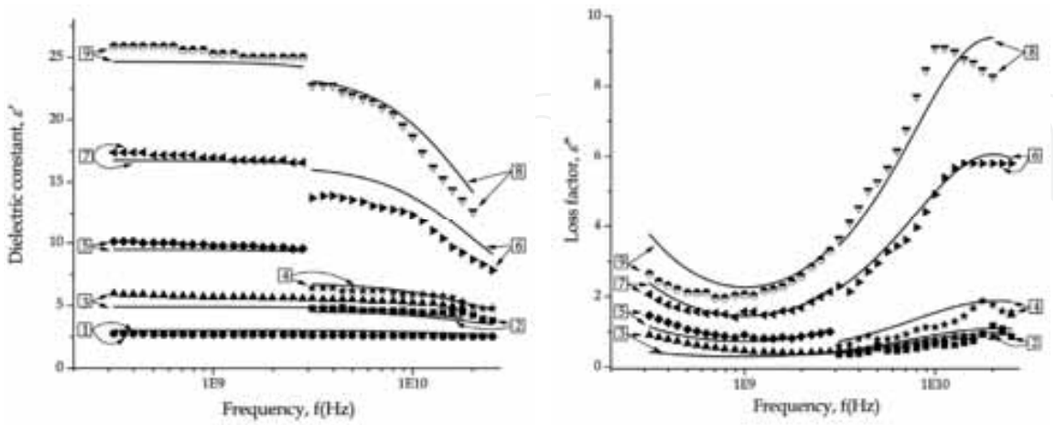

Fig. 6. DC, ε', and LF, ε'', spectra for soil D measured (dots) and fitted (solid line) with the use of the GRMDM model.. Shown data correspond to the following soil volumetric moistures, *W(%)*: 1) 3.2; 2) 8; 3) 8.8; 4) 13.2; 5) 18.4; 6) 29.1; 7) 29.7; 8) 38.2; 9) 39.4

With this technique of fitting, the FD RMDM spectroscopic parameters were attained for the whole set of soils listed in Table 3. Thus obtained, the FD RMDM parameters are shown with symbols in Figure 7 as functions of clay content.

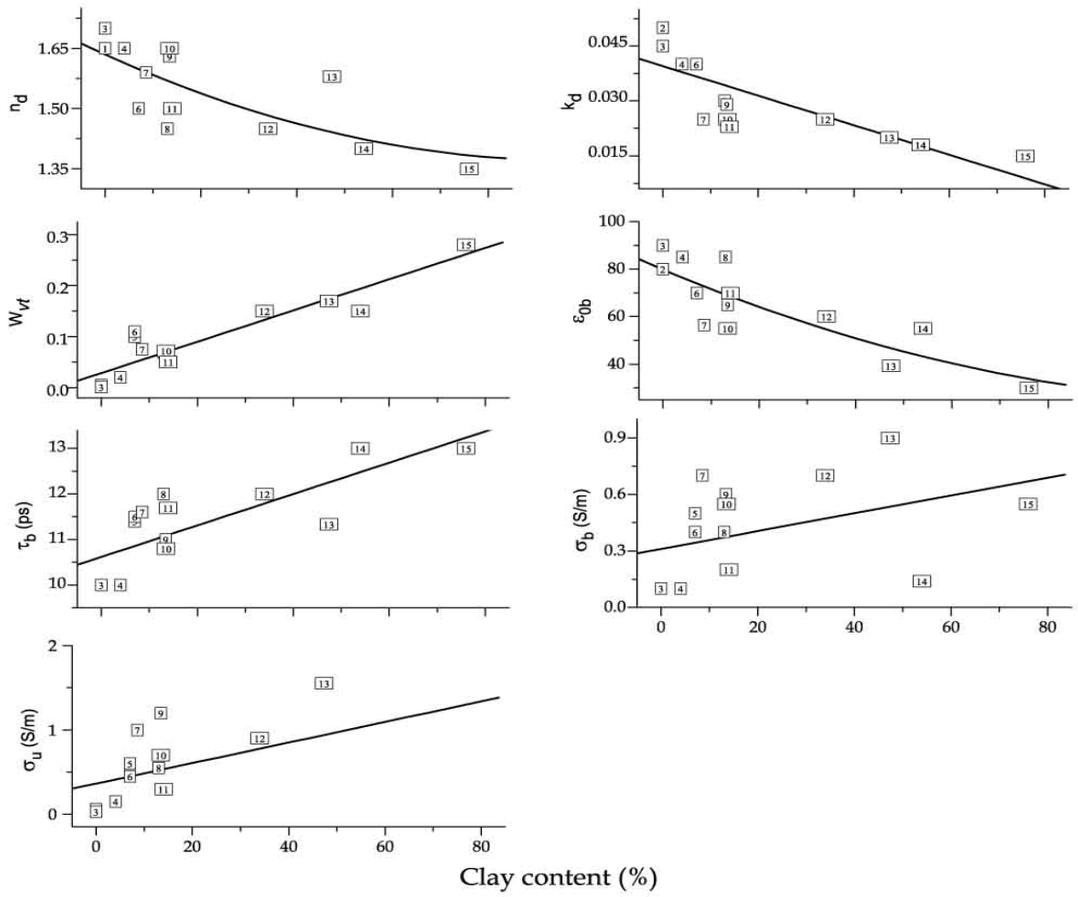

Fig. 7. The GRMDM spectroscopic parameters for the soils presented in Table 1 as a function of gravimetric clay content. The squares represent values derived through fitting the dielectric spectra. The numbers shown in squares correspond to those given in Table 3.

To estimate the error of the FD RMDM predictions for the DCs and LFs over this ensemble of soils, there were applied equations (3), (4), (12), (13), (22), (23) in conjunction with the FD RMDM spectroscopic parameters given in Figure 7. The measured DCs and LFs versus the predicted ones are demonstrated in Figure 8, with the error of prediction being given in the figure caption. According to Figure 8, the error in terms of standard deviation, correlation coefficient and squint of the linear regression with regard to 1 to 1 line appeared to be quit acceptable, given a wide domain of frequencies, soil textures, and moistures.

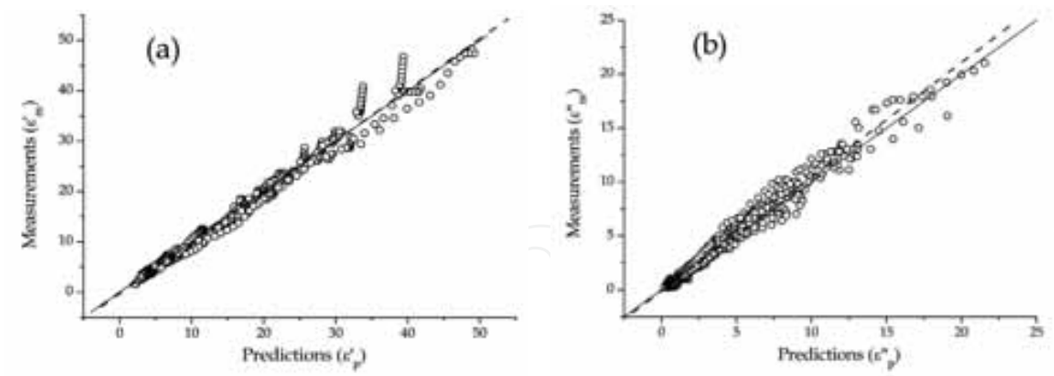

Fig.8. Correlation of the FD RMDM predictions, ε'_p, ε''_p, for DCs (a) and LFs (b) with the measured ones, ε'_m, ε''_m, in the case of soils measured in (Curtis et al., 1995). Solid and dotted lines represent bisectors and linear fits, respectively. Correlation coefficients, R_{DC} and R_{LF}, and standard deviations, SD_{DC} and SD_{LF}, are equal to: R_{DC}=0. 995, R_{LF}=0.991, SD_{DC}=1.023, SD_{LF}=0.4899.The linear fits are expressed as follows: ε'_m=-0.2753 + 1.013 ε'_p, ε''_m=-0.0943 + 1.058 ε''_p.

Generalizing the above analysis, it is possible to assert that the FD RMDM, having been adjusted to each specific soil, as in Figure 6, can ensure acceptable accuracy of dielectric predictions. This result makes possible to use the FD RMDM as a building block to create a frequency and texture dependable dielectric model (FTD RMDM) for moist soils. For this purpose, the whole set of FD RMDM parameters in Figure 7 was fitted with the functions of clay percentage (Mironov et al., 2009a), yielding the equations given in Table 4.

n_d=1.634-0.539·10^{-2}C+0.2748·10$^{-4}C^2$	ε_{0b} =79.8-85.4C+32.7·10$^{-4}C^2$	ε_{0u} =100
k_d=0.03952-0.04038·10^{-2}C	τ_b =1.062·10^{-11}+3.450·10^{-12}·10^{-2}C	τ_u =8.5·10^{-12}
W_t=0.02863+0.30673·10^{-2}C	σ_b =0.3112+0.467·10^{-2}C	σ_u =0.3631+1.217·10^{-2}C

Table 4. Fits for the FD RMDM as a function of clay percentage

The clay content, C, and relaxation times, τ_b and τ_u, in the formulas of Table 4 are expressed in percentages and seconds, respectively. Further on, the equations in Table 4 are referred to as the FTD RMDM fits, while the values calculated with these equations will be identified as the FTD RMDM spectroscopic parameters. Finally, the DCs and LFs calculated with formulas (3), (4), (12), (13), (22), (23) in conjunction with the spectroscopic parameters given in Figure 7 are identified as the FTD RMDM dielectric predictions. Clay percentage, C, is the only input parameter of the FTD RMDM in terms of soil texture to account for a specific type of soil. It should be especially noticed that the equations in Table 4 generalize all the information presented in Figure 7 on the FD RMDM spectroscopic parameters regarding the 15 soils of Table 3.

The same correlation analysis, as shown in Figure 8 in the case of the FD RMDM, was conducted with respect to the FTD RMDM. It proved the FTD RMDM prediction errors to be on the same order as those given in Figure 8. This result signifies that, over the whole variety of soil types, moistures, and frequencies measured in (Curtis et al., 1995) and (Hallikainen et al., 1985; Dobson et al. 1985) the FTD RMDM can predict the DCs and LFs

with the same accuracy, in terms of correlation coefficient and standard deviation, as the FD RMDM does.

Nevertheless, it is worth mentioning that the FTD RMSD prediction error has been tested only over the dielectric data, which were used for its developing. In case the test is carried out regarding the dielectric data with which a respective regression model is created, it can reveal only an error of regression analysis itself, as was done in (Wang&Schmugge, 1980; Dobson et al. 1985). To verify an intrinsic predictive power of the FTD RMDM, it has to be tested over the dielectric data set other than the one used for deriving formulas like in Table 4. To perform such a validation of the FTD RMDM, the formulas in Table 4 were obtained, first, with the use of spectroscopic parameters relating to all the soils excluding the ones coded as F1, F2, F3, and F5 and, second, only with the use of soils F1, F2, F3, and F5. As a result, these two new versions of the FTD RMDM could be treated as independent with regard to the soil sets which were not used in their developing. Then the tests like that in Figure 8, were conducted for the both FTD RMDM versions with respect to the DC and LF data independently measured. With these tests, the errors for both FTD RMDM versions was found (Mironov et al., 2009a) to be on the same order as the ones seen in Figure 8. In addition, we have tested the FTD RMDM against the independently measured dielectric data, which are available in (Wang&Schmugge, 1980; Sabburg et al. 1997; Mironov et al., 2004; 2005; 2006), finding the error of the FTD RMDM predictions to be on the same order as that in Figure 8 is.

As seen in Figure 9 borrowed from (Mironov et al., 2009a], in contrast to the physically based FTD RMDM, the regression model of (Dobson et al., 1985) provided for DC and LF predictions with considerably greater error than that observed in Figure 8, pertaining to the FTD RMDM.

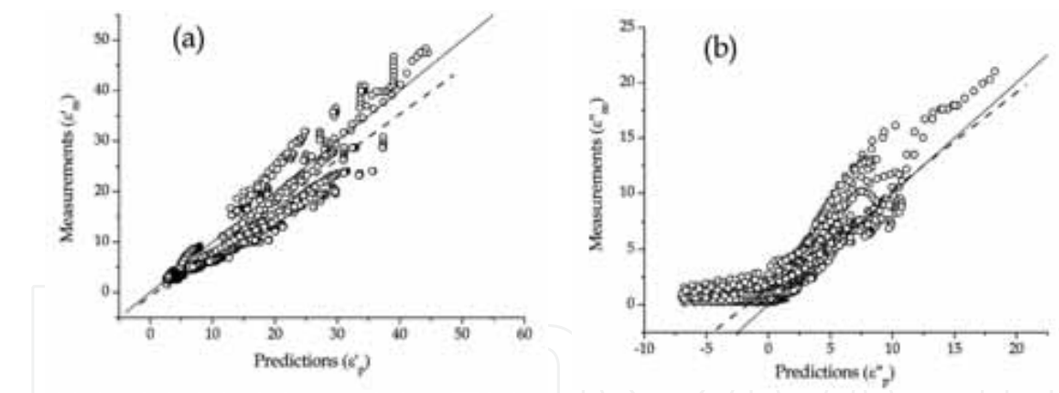

Fig.9. Correlation of the semiempirical model (Dobson et al. 1985) predictions, ε'_p, ε''_p, for DCs (a) and LFs (b) with the measured ones, ε'_m, ε''_m, in the case of soils measured in (Curtis et al.,1995). Solid and dotted lines represent bisectors and linear fits, respectively. Correlation coefficients, R_{DC} and R_{LF}, and standard deviations, SD_{DC} and SD_{LF}, are equal to: R_{DC}=0.942, R_{LF}=0.882, SD_{DC}=3.391, SD_{LF}=1.695. The linear fits are expressed as follows: ε'_m=-0.753 + 0.902ε'_p, ε''_m=1.483 + 0.881ε''_p.

It is worth noting here that the methodology employed for developing the FTD RMDM is based on two key elements. The first one is the FD RMDM, which ensures accurate dielectric predictions using a cluster of the FD RMDM, parameters pertaining to the respective cluster of soil types with specific textures. The second key element is the completeness of such soil

clusters in terms of texture diversity. An example of such a cluster is shown in Figure 7. Within the FTD RMDM methodology, the cluster of the FTD RMDM parameters pertaining to a specific ensemble of soils is turned into a specific collection of the regression equations given in Table 4, which represent the example of a specific version of the FTD RMDM related to the ensemble of soils listed in Table 4. The more complete ensemble of soils is available the less error of prediction with the respective version of the FTD RMDM can be attained, especially in regard with the soils other than those used to develop the particular version of the FTD RMDM. Therefore, the FTD RMDM prediction error, regarding the whole variety of natural soils, must depend on both the predictive capability of the FD RMDM, which is a physically based building block of the FTD RMDM, and the completeness of the ensemble of soils employed, in terms of diversity of their texture, which is a regression analysis building block of the respective version of the FTD RMDM. The more complete such a data set is the less regression analysis error in the equations similar to those given in Table 4 can be obtained, thus ensuring less error of predictions related to the respective FTD RMDM version.

One more problem regarding the FTD RMDM prediction error needs to be discussed. It concerns the question whether the FTD RMDM trained on a specific variety of soils is able to provide for dielectric spectra (22), (23) to the data measured predictions in the case of an individual soil, which belong to that variety. Let us consider such a situation. In Figure 10, experimental DCs and LFs are plotted versus the FTD RMDM predictions in the case of specific soil D measured in (Curtis et al., 1995). At that, in Figure 10, there was used the version of FTD RMDM based on the formulas from Table 4, which correspond to the whole variety of soils listed in Table 1. The data predicted with the FTD RMDM instead of the initial FD RMDM parameters as shown in Figure 6, appeared to follow the measured ones quite well for DCs and good enough in the most cases for LFs, excluding the data for greater moistures (graphs 7 and 9) in the range of frequencies below 2 GHz. As seen in Figure 7, this deviation arises from a noticeable difference between the free water conductivities derived with the FD RMDM fitting technique and calculated with the FTD RMDM formulas of Table 4.

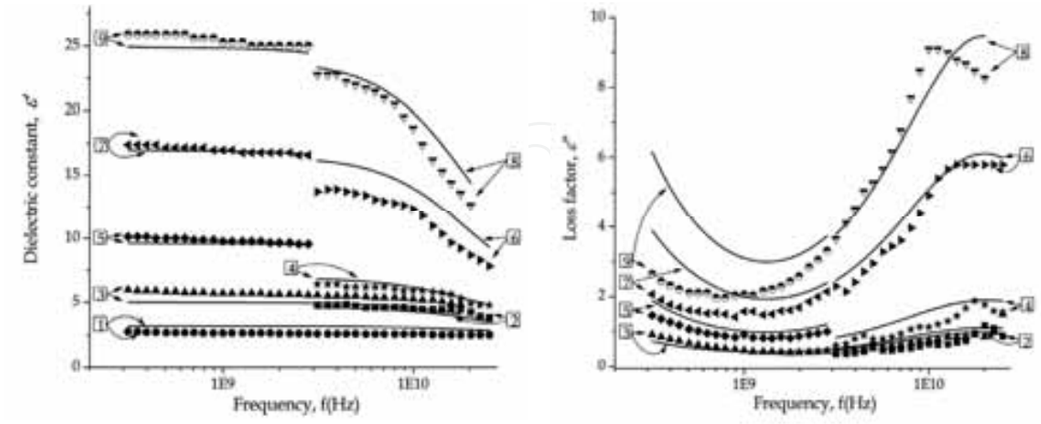

Fig. 10. DC, ε', and LF, ε″, spectra for soil D measured (dots) and calculated with the use of FTD RMDM (solid lines). Shown data correspond to the following soil volumetric moistures, W(%): 1) 3.2; 2) 8; 3) 8.8; 4) 13.2; 5) 18.4; 6) 29.1; 7) 29.7; 8) 38.2; 9) 39.4

As seen from Figures. 6 and 10, the error of prediction in the case of an individual soil D, with the FTD RMDM trained on a composite variety of soils listed in Table 3 is on the same order as the one obtained with the use of the FD RMDM (Figure 6) is, the latter being trained specifically on dielectric data from (Curtis et al., 1995) pertaining to soil D. As a result, it can be stated that the physically based FTD RMDM has demonstrated noticeably less prediction error, compared to the regression dielectric model of (Dobson et al., 1985), in the case of both a group of soils or an individual soil. falling out of the varieties of soils used to develop respective models.

6. Conclusions

Summing up the results, the following has to be stated as primary findings of this research.
First, the physical law describing both the index of refraction and attenuation coefficient as a function of moisture content has been substantiated. This law has a form of the well known refractive mixing dielectric model, with the index of power being equal to 0.5, regarding the complex dielectric constants of the components mixed.
Second, the bound and free soil water dielectric spectra were shown to follow the Debye relaxation law. The technique to derive the high and low frequency limits of dielectric constant, relaxation time, and conductivity for both type of soil water has been proposed and tested.
Third, there was confirmed ability for the frequency dependent refractive mixing dielectric model recently developed in (Mironov et al., 2004) to generate good dielectric predictions over the ensemble consisting of 15 natural soils having the textures covering almost all natural soils. These predictions proved to be accurate, concerning the frequency range from 0.3 to 26.5 GHz, volumetric moistures spanning from nearly dry condition to field capacity moistures, with the temperatures being of from 20 to 22○C. This model has error about three times as small with regard to model which is currently employed in practice of the geoscience and remote sensing.
Forth, the frequency dependent refractive mixing dielectric model was generalized. As a result the frequency and texture dependent refractive mixing dielectric model for moist soils, which proved to provide for complex dielectric constant spectra predictions with error on the same order as the frequency dependent refractive mixing dielectric model does. At that, the soil clay percentage is the only input parameter in terms of soil texture for the frequency and texture dependent refractive mixing dielectric model.

7. Future work

The results discussed in this chapter are applicable only in the narrow range of temperatures from 20 to 22^{o}, in which the dielectric data were attained (Dobson et al. 1995; Curtis et al., 1995). To extend these results over a larger range of temperatures, a temperature and frequency dependent refractive mixing dielectric model must be developed, as in (Mironov et al., 2009a), to become a building block for a temperature and texture dependent refractive mixing dielectric mode, the first approach to which has already been made in (Mironov&Fomin, 2009). There is also a lot of work to be done regarding the tests of the dielectric models developed over the existing dielectric data and radar and radio

thermal remote sensing data available in the literature. This must help define the domains of their applicability in the practice of geoscience and remotes sensing.

8. Acknowledgements

This work is supported by the Siberian Branch Russian Academy of Sciences under project No. 2.5.1.1: "Dielectric spectroscopy of natural media in the radio frequencies band." (2007-2011). The authors would also like to express gratitude to their colleagues Lyudmila Kosolapova, Sergej Fomin, Yurij Lukin, and Igor Savin for processing a great many of dielectric data and preparing some figures and tables, when developing this paper for publication. As well as the Russian Foundation for Basic Research under project No. 09-05-91061: "Development of a soil dielectric constant model." (2009-2011).

9. References

Birchak, J. R.; Gardner, C. G.; Hipp, J. E. & Victor, J. M. (1974). High dielectric constant microwave probes for sensing soil moisture, Proc. IEEE, Vol. 62, No. 1, January 1974 pp. 92-98.

Curtis, J.O.; Weiss, C.A. Jr. & Everett, J.B. (1995). Effect of Soil Composition on Dielectric Properties, Technical Report EL-95-34, U.S. Army Corps of Engineers, Waterways Experimental Staton, Vicksburg, MS, December 1995.

Dobson, M. C.; Ulaby, F. T.; Hallikainen, M. T. & El-Rayes, M. A. (1985). Microwave dielectric behavior of wet soil: Part II – Dielectric mixing models, IEEE Trans. Geosci. Remote Sensing, Vol. 23, No. 1, January 1985 pp. 35-44.

Hasted, J. B. (1973). Aqueous Dielectrics, Chapman and Hall, London.

Hallikainen, M. T.; Ulaby, F. T.; Dobson, M. C.; El-Rayes, M. A. & Lin-Kun-Wu. (1985). Microwave dielectric behavior of wet soil: Part I – Empirical model and experimental observations, IEEE Trans. Geosci. Remote Sensing, Vol. 23, No. 1, January 1985 pp. 25-34.

Komarov, S. A. & Mironov, V. L. (2000). Microwave Remote Sensing of Soils, Publishing House of the Siberian Branch of the Russian Academy of Sciences, Novosibirsk, Russia.

Lukin, Yu. I.; Mironov, V.L. & Komarov, S.A. (2008). Investigation of dielectric spectra from moist soils during freezing-thawing processes. Russian Physics Journal, Vol. 51, No. 9, September 2008 pp. 907-911, ISSN 1064-8887.

Mironov, V. L.; Komarov, S .A.; Rychkova, N. V. & Kleshchenko, V. N. (1995). Study of the Dielectric Properties of Wet Grounds at Microwave Frequencies, Earth Obs. Rem. Sens., Vol. 12, No. 4, April 1995 pp. 495-504.

Mironov V. L.; Dobson, M. C.; Kaupp, V. H.; Komarov, S. A. & Kleshchenko, V. N. (2002). Generalized refractive mixing dielectric model for moist soils, Proceedings of IGARSS'02, Vol.VI, pp. 3556-3558, Toronto, Canada.

Mironov, V.L. & Bobrov, P.P. (2003). Soil Dielectric Spectroscopic Parameters Dependence on Humus Content, Proceedings of IGARSS'03, Vol. II, pp. 1106-1108, Toulouse, France.

Mironov, V.L. (2004). Spectral Dielectric Properties of Moist Soils in The Microwave Band, Proceedings of IGARSS'04, Vol. V, pp. 3474 – 3477, Anchorage, USA.

Mironov, V.L.; Dobson, M. C.; Kaupp, V. H.; Komarov, S. A. & Kleshchenko, V. N. (2004). Generalized refractive mixing dielectric model for moist soils, IEEE Trans. Geosci. Remote Sensing, Vol.42, No.4, April 2004 pp. 773–785.

Mironov V.L.; Bobrov, P.P.; Bobrov, A.P.; Mandrygina V.N. & Stasuk V.D. (2005). Microwave Dielectric Spectroscopy of Moist Soils for a Forest-tundra Region, Proceedings of IGARSS'05, Vol. V, pp. 4485-4488, Seoul, Korea.

Mironov V.L.; Bobrov, P.P.; Kosolapova, L.G.; Mandrygina, V.N. & Fomin S.V. (2006). Data Processing Technique for Deriving Soil Water Spectroscopic Parameters in Microwave Range, Proceedings of IGARSS'06, Vol. VI, pp. 2957-2961, Denver, USA.

Mironov, V.L.; Savin, S.V. & Roo R.D. (2007). Dielectric Spectroscopic Model for Tussock and Shrub Tundra Soils, Proceedings of IGARSS'07, July 2007 pp. 726–731, Barcelona, Spain.

Mironov, V.L.; Kosolapova, L.G. & Fomin, S.V. (2009a). Physically and mineralogically based spectroscopic dielectric model for moist soils, IEEE Trans. Geosci. Remote Sensing, Vol.47, No.7, Part 1, July 2009, pp.2059 - 2070.

Mironov V.L. & Fomin S.V. (2009b). Temperature Dependable Microwave Dielectric Model for Moist Soils, Proceedings of PIERS 2009, March 23-27 2009 pp. 831-835, Beijing, CHINA.

Miyamoto, T. & Chikushi, J. (2006). Time domain reflectometry calibration for typical upland soils in Kyushu (Japan), JARQ, Vol. 40, No. 3, 2006 pp.225-231, http://www.jircas.affrc.go.jp.

Peplinski, N. R.; Ulaby, F. T. & Dobson, M. C. (1995a). Dielectric properties of soils in the 0.3-1.3-GHz range, IEEE Trans. Geosci. Remote Sensing, Vol. 33, No. 3, March 1995 pp. 803-807.

Peplinski, N.A.; Ulaby, F.T. & Dobson, M.C. (1995b). Correction to Dielectric properties of soils in the 0.3-1.3 GHz range, IEEE Trans. Geosci. Remote Sensing, Vol. 33, No. 6, June 1995 pp.1340.

Rychkova, N. (1997). Investigation of Radiophysical Properties of Soil with regard to Remote Sensing Problems, Ph.D. Thesis, Alatai State University, Russia.

Sabburg, J.; Ball, J. A. R. & Hancock, N. H. (1997). Dielectric behavior of moist swelling clay soils at microwave frequencies. IEEE Trans. Geosci. Remote Sensing, Vol. 35, No. 1, January 1997 pp. 784-787.

Stogryn, A. (1971) Equations for Calculating the Dielectric Constant of Saline Water IEEE Transactions on Microwave Theory and Techniques, Volume 19, Issue 8, Aug 1971 Page(s):733 - 736

Ulaby, F. T.; Moor, R. K. & Fung A. K. (1986). Microwave Remote Sensing, Active and Passive, vol. III, Artech House, Dedham, MA.

Wang, J. & Shmugge, T. (1980). An empirical model for the complex dielectric permittivity of soils as a function of water content. IEEE Trans. Geosci. Remote Sensing, Vol. 18, No. 4, April 1980 pp. 288-295.

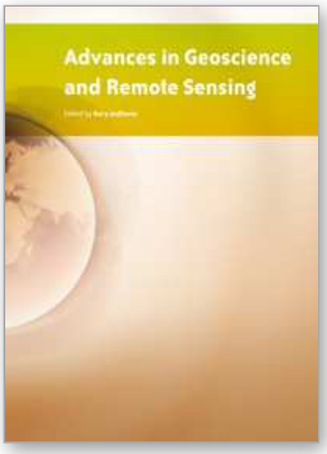

Advances in Geoscience and Remote Sensing

Edited by Gary Jedlovec

ISBN 978-953-307-005-6

Hard cover, 742 pages

Publisher InTech

Published online 01, October, 2009

Published in print edition October, 2009

Remote sensing is the acquisition of information of an object or phenomenon, by the use of either recording or real-time sensing device(s), that is not in physical or intimate contact with the object (such as by way of aircraft, spacecraft, satellite, buoy, or ship). In practice, remote sensing is the stand-off collection through the use of a variety of devices for gathering information on a given object or area. Human existence is dependent on our ability to understand, utilize, manage and maintain the environment we live in - Geoscience is the science that seeks to achieve these goals. This book is a collection of contributions from world-class scientists, engineers and educators engaged in the fields of geoscience and remote sensing.

InTech Europe
University Campus STeP Ri
Slavka Krautzeka 83/A
51000 Rijeka, Croatia
Phone: +385 (51) 770 447
Fax: +385 (51) 686 166
www.intechopen.com

InTech China
Unit 405, Office Block, Hotel Equatorial Shanghai
No.65, Yan An Road (West), Shanghai, 200040, China
中国上海市延安西路65号上海国际贵都大饭店办公楼405单元
Phone: +86-21-62489820
Fax: +86-21-62489821

IntechOpen